Fusion-born Alpha Particle Ripple Loss Studies in ITER

G.J. Kramer[1], R.B. White[1], R. Nazikian[1], and H.L. Berk[2]

[1] *Princeton Plasma Physics Laboratory, Princeton, NJ 08543, U.S.A.*
[2] *Institute for Fusion Studies, Austin, Texas, 78712*

e-mail: gkramer@pppl.gov

Abstract Fusion-born alpha particle losses are investigated for two ITER scenarios with and without test blanket modules (TBMs). When the TBMs were present it was found that the losses increased by a factor of two overall with a marked increase in its localization. The heat load on the first wall with optimized ripple (0.2%) and no TBMs was spread uniformly over the outer wall due to the 18-fold symmetry of the toroidal field coil set. In the simulations with the TBMs three intense hot spots were obtained with heat loads up to 0.7 MW/m^2 in front of the TBMs.

1 Introduction

Alpha particles in ITER should be confined well during the burn phase of the discharge and not lost due to the effects of magnetic field ripple. Alpha particle losses have been studied in the past in order to obtain the heat load on plasma facing components due to ripple induced losses [1, 2]. In previous ITER studies it was found that when the toroidal field ripple was kept below 0.2% at the last closed flux surface (LCF), by use of ferritic inserts between the inner and outer shell of the vacuum vessel, heat loads due to fusion born alpha particles where well within the required limits for various plasma scenarios.

A major goal on ITER is to study tritium breeding in blanket modules. Three test blanket modules (TBMs) are being envisioned for ITER. These TBMs will be inserted at the mid-plane at three toroidal angles, -40, 0, and 40 deg. and they have a significant impact on the toroidal field ripple as can be seen in fig. 1b and c. The 18-fold toroidal symmetry is broken and three strong magnetic perturbations are created in front of the TBMs that affect the fusion-born alpha particle confinement negatively by creating three localized hot spots with heat loads up to 0.7 MW/m^2 in front of the TBMs (section 4).

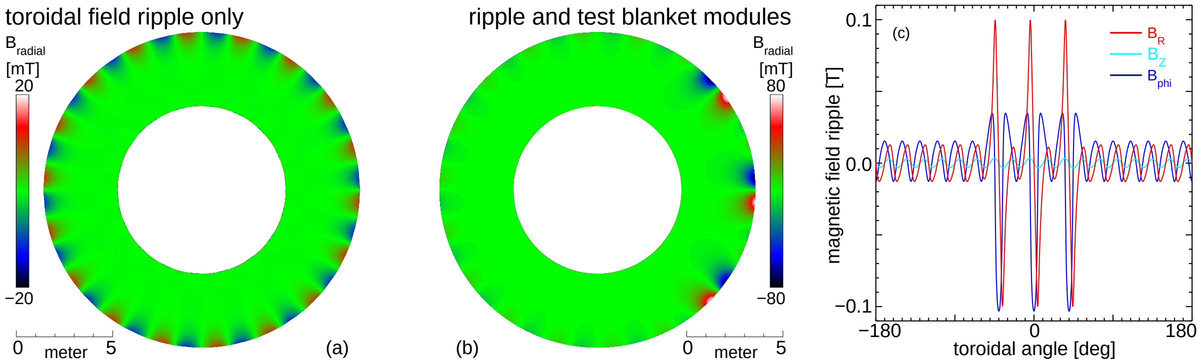

Figure 1: *Radial component of the ITER toroidal field ripple without (a) and with (b) the three TBMs and (c) the radial, vertical and toroidal magnetic field components at the LCF mid plane at R=8.28 m and Z=0.60 m. Note the four fold increase of the color scale between (a) and (b).*

In this study we have examined for two standard ITER configurations: Scenario 2 an inductive 15 MA plasma producing 400 MW of fusion power with Q=10 for 400 s, and Scenario 4 a 9 MA steady state weakly reversed magnetic shear plasma producing 300 MW of fusion power with Q=5 for 3000 s (section 2). In both cases ripple-induced fusion-born alpha particle losses were calculated with and without the three TBMs (section 4).

The loss calculations were performed with the ORBIT and SPIRAL codes [3, 4]. The ORBIT code is a guiding center following code whereby the field ripple is given as a sum over a few toroidal harmonics and was used to study the cases without TBMs. The SPIRAL code uses the Lorenz force to follow the full particle orbit in a toroidal magnetic field configuration with arbitrary ripple (section 3). From the simulation results it is concluded that the toroidal field ripple due to the TBMs can be harmful for the first wall.

2 equilibrium configurations

We have examined the fusion-born alpha particle losses for two standard ITER configurations, Scenario 2 (fig. 2a and c) an inductive 15 MA plasma producing 400 MW of fusion power with Q=10 for 400 s, and Scenario 4 (fig. 2b and c) a 9 MA steady state weakly reversed magnetic shear plasma producing 300 MW of fusion power with Q=5 for 3000 s. In both cases the losses were calculated with the toroidal field ripple, with and without the three TBMs. Those equilibrium configurations together with the alpha particle birth distribution (fig. 2d) were obtained from the ITER data base [5].

The 3-D magnetic ripple fields were obtained from G. Sabiene [6]. In fig. 1 the radial component of the ripple field is shown without and with the TBM ripple field included. For the toroidal field ferritic inserts were included to reduce the toroidal field ripple at the plasma edge to 0.2% from well over 1% without ferritic inserts. The TBMs that were used in the magnetic field calculations consisted of two equal modules of 2.1 ton ferritic steel (EUFER), stacked vertically, and placed in one equatorial port. Three ports, at -40, 0, and 40 deg. toroidal angle were loaded with TBMs in our simulations. The three components of the magnetic field ripple due to the TBMs are shown in fig. 1c at the low field-side plasma mid plane.

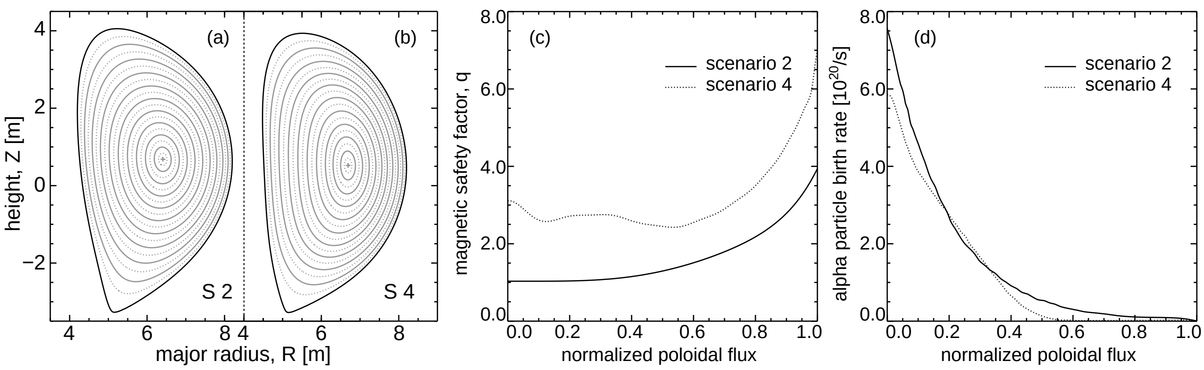

Figure 2: *ITER equilibrium plasma configurations for scenario 2 (a) and scenario 4 (b) with equispaced minor radius contours indicated. The magnetic safety factor profiles and Alpha-particle birth distributions are shown in (c) and (d) respectively.*

3 simulations

The fusion-born alpha particle loss calculations were performed with the ORBIT and SPIRAL codes. The ORBIT code is a guiding center following code whereby the field ripple is given as a sum over a few toroidal harmonics and was used to study the cases without TBMs. The ORBIT code is well documented and a description of the code can be found in [3, 4]. In both the ORBIT and SPIRAL code fusion-born alpha particles were drawn from the alpha-particle birth distributions (fig. 2d) and followed for a certain amount of time after their birth (up to 40 ms in the ORBIT code and 2 ms in the SPIRAL code) When the particle passed the LCF it was marked as lost.

The SPIRAL code was developed recently to study ripple fields that cannot be decomposed in one or a few dominant toroidal components such as the ITER ripple field with TBMs. It uses the full Lorentz force to calculate the particle orbits. A toroidally symmetric equilibrium magnetic field which contains the contributions of the plasma was obtained from an EFIT calculation. EFIT gives the deviation of the toroidal magnetic field as function of the major radius, R, from the ideal field: R_0B_0/R, with B_0 the toroidal magnetic field at R_0 while the vertical and radial fields are obtained from the poloidal flux function, $\Psi_p(R,Z)$, (Z the vertical coordinate). This flux function is given on a rectangular grid with a resolution of approximately 2 cm. For the particle orbit calculations Ψ_p has to interpolated in between the grid points in an accurate and fast way. This was achieved as follows. The poloidal flux function was decomposed into a double sum of Chebychev polynomials of the first kind, $T(x)$, [7]:

$$\Psi_p(R,Z) = \sum_i \sum_j a_{ij} T_i(R) T_j(Z) \tag{1}$$

and usually about 30 terms are kept for each sum to give a maximum deviation of less that 0.5% between the given points and the polynomial expansion. The radial (B_R) and vertical (B_Z) magnetic fields are then obtained by taking the derivatives of eq. 1 with respect to R and Z:

$$\begin{aligned} B_R &= \frac{1}{R}\frac{\partial \Psi_p(R,Z)}{\partial Z} = \frac{1}{R}\sum_i \sum_j a^z_{ij} T_i(R) T_j(Z) \\ B_Z &= -\frac{1}{R}\frac{\partial \Psi_p(R,Z)}{\partial R} = -\frac{1}{R}\sum_i \sum_j a^r_{ij} T_i(R) T_j(Z) \end{aligned} \tag{2}$$

whereby taking the derivatives of the Chebychev polynomials is obtained by rearangeing the coefficients a_{ij} into a^r_{ij} (a^z_{ij}) for the radial (vertical) field. It can be shown that that the equilibrium magnetic field constructed in this way is guaranteed divergence free as required by Maxwells equations.

The toroidal ripple fields [6] that we have used in our calculations were specified as $(\tilde{B}_R, \tilde{B}_\varphi, \tilde{B}_Z)$ at 432 equally spaced toroidal angles on 1436 locations in each RZ-plane. These ripple fields were calculated for the vacuum field only. For fast and accurate calculations we have expanded the $\tilde{B}_R$ and $\tilde{B}_Z$ components of the ripple field into finite Chebychev sums similar to the equilibrium field. For the interpolation in the toroidal direction we have used a quadratic polynomial around each toroidal planes:

$$\tilde{B}^i_x(R,\varphi,Z) = \tilde{B}^i_x(R,Z) + U^i_x(R,Z)\varphi + V^i_x(R,Z)\varphi^2 \tag{3}$$

(with x either R or Z, and i the index of the i^{th} plane) and demanded that the radial and vertical fields and their derivatives are continous half way between two given planes. After

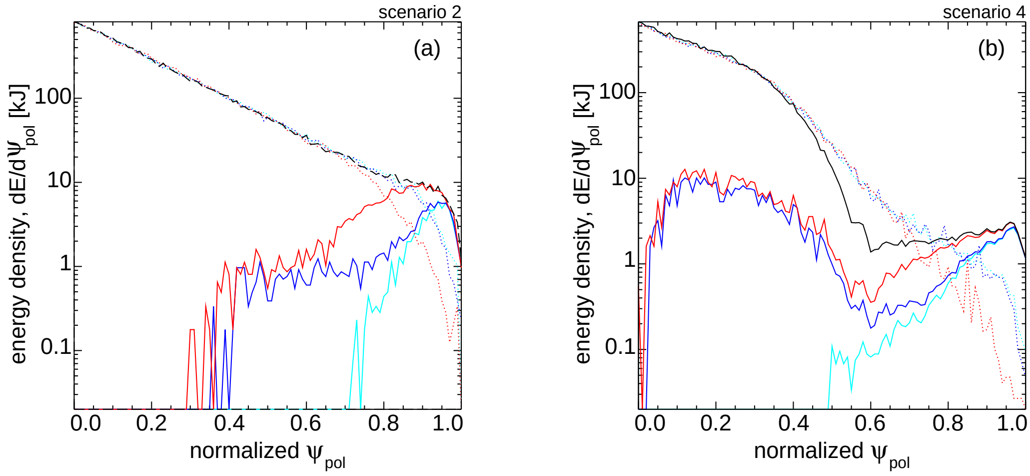

Figure 3: *Lost alpha particle energy in 2 ms for scenario 2 (a) and scenario 4 (b) calculated with the SPIRAL code. Solid curves: losses for the equilibrium field without ripple and TBMs (cyan), field ripple only (blue), and field ripple and TBMs (red). the solid black curve is the birth profile while the dotted curves are the alpha particle profiles after 2 ms (same color coding as the loss profiles).*

expanding the functions $\tilde{B}_x^i(R,Z)$, $U_x^i(R,Z)$, and $V_x^i(R,Z)$ into a finite sum of Chebychev polynomials (In the current calculations 10 coefficients in the radial and 15 in the vertical direction were sufficient to describe the ripple fields accurately) the expansion coefficients can be determined uniquely from the condition that the fields should be periodical in φ. From the condition that the magnetic field should be divergence free the poloidal component was calculated. This involved differentiating the expansions of $\tilde{B}_x^i$, U_x^i, and V_x^i with respect to R and Z summing the various components and integrating with respect to φ. All those operations were performed analytically using the Chebychev expansion coefficients and therefore, the ripple field is also guaranteed to be divergence free in the calculations down to the numerical precision of the computation. The analytically constructed $\tilde{B}_\varphi$ field was in excellent agreement with the given numerical one [6].

The differential equation solver that is used in the SPIRAL code is a NAG implementation [9] of a variable-order, variable-step, Adams method integrator [8]. A key feature of this integrator is that the user gives the time interval over which the equations are to be integrated together with the desired accuracy at the end of the integration. The algorithm then determines the number of steps to be taken to obtain the requested accuracy, in our case up to ten million evaluations were performed for following the particles for 2 ms. For our runs we have set the accuracy in such a way that the average particle energy was conserved by better than 0.1% with similar values for the magnetic moment. In order to access the effects of the accuracy we have performed one run in which the energy was conserved to four parts per million at the expense of a a four-fold increase in CPU time and like wise in the number of evaluations. The losses that were found in this case and the distribution at the LCF were very similar, thereby justifying the chosen setting of the accuracy parameter.

4 Results

The alpha particle birth rate is strongly peaked toward the plasma center (fig. 2d) while the main losses occur near the edge (fig. 3). In order to sample the edge region with

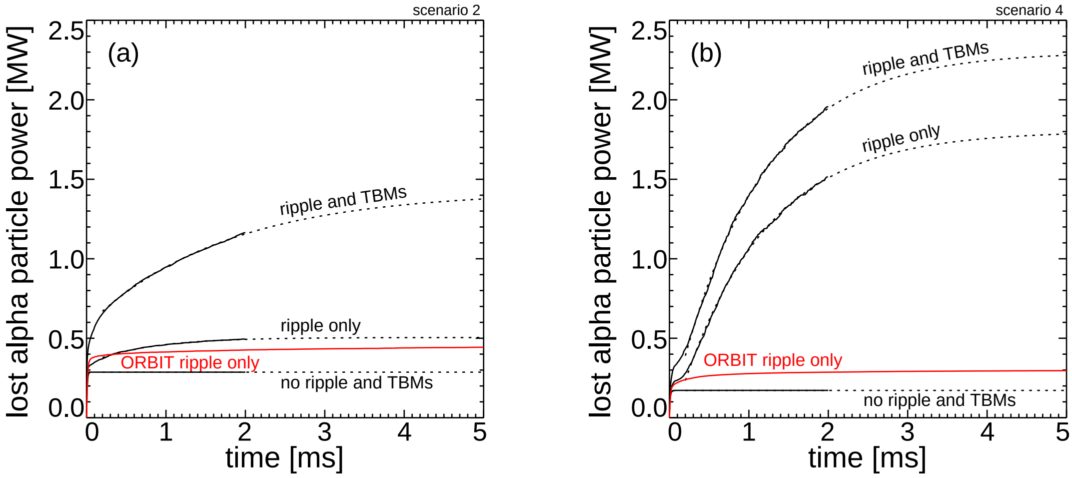

Figure 4: *Lost alpha particle power as function of time after birth for scenario 2 (a) and scenario 4 (b) for the equilibrium field without ripple and and TBMs, ripple only, and ripple and TBMs. The solid curves are obtained from the SPIRAL code while the dashed curves are exponential extrapolations.*

high statistical accuracy in our Monte Carlo simulations, three separate runs were performed where the particles were distributed in three plasma shells from $\Psi_{\mathrm{pol}} = [0.0, 0.25]$, $[0.25, 0.50]$, and $[0.50, 1.0]$ according to the alpha particle birth profiles and spread uniformly over the flux surface and pitch angle. In each shell 20000 particles were used to follow the orbits for up to 2.0 ms. Afterward, the results from the three regions were combined for further analysis and the numbers of lost particles are transformed into lost power.

From the results of the SPIRAL code, shown in fig. 3a, it can be seen that the losses for scenario 2 come mainly from the outer layers of the plasma well beyond $\Psi_{\mathrm{pol}} = 0.5$ (or $r/a = 0.6$) and that the extra losses due to the the TBMs occur also in that region. For scenario 4 alpha particles are lost over a much larger region, nearly up to the plasma center, when either toroidal field ripple alone or toroidal field ripple and TBMs are included (fig. 3b). Enhanced losses due to the TBMs come from both the edge and to a lesser extend from the core.

Particles should be followed long enough so that they reach the LCF. One way to investigate weather the integration time is sufficient is to plot the accumulated losses as a function of time as shown in fig. 4 and investigate if the losses saturate. From this figure it can be seen that after 2 ms not all the particles are lost. For calculating heat loads it is important to use the total losses and not the losses found in the simulations with a finite run time. The loss rate can well be described by a decaying exponential $(a + b(1 - \exp(-t/\lambda))$ and therefore, we have fitted an exponential to the loss curves obtained in the simulations curves where we have used the time interval from 0.2 to 2 ms to avoid interference from the prompt losses which occur on time scales of less than 100 μs. The loss times, λ, that were found for scenario 2 were 0.7 ms without TBMs and 1.7 ms with TBMs. For scenario 4 a decay constant of 1.1 ms was found for the ripple case without or with TBMs. The losses occur on a much faster time scale that the slowing down time which is 1.5 s for scenario 2 and 2.1 s for scenario 4, justifying the choice not to include slowing down effects in the present calculations.

In fig.4 the lost power as calculated using ORBIT for the toroidal coil field ripple only case is also shown. For scenario 2 the ORBIT and SPIRAL codes agree well but for scenario 4 the SPIRAL code finds much higher losses than ORBIT even without

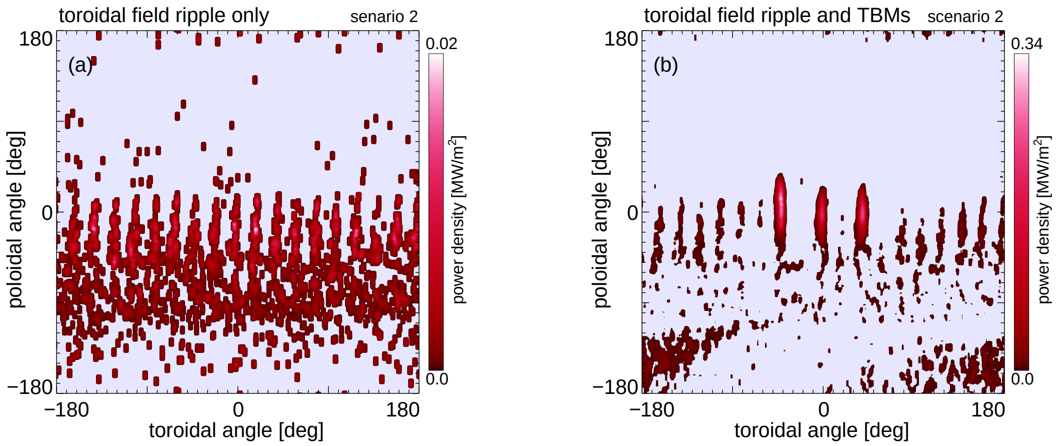

Figure 5: *calculated heat loads for scenario 2 at the LCF with field ripple only (a) and field ripple and TBMs (b). Note the seventeen fold increase in the power density scale in (b).*

TBMs. The (guiding-center following) ORBIT results are consistent with losses calculated from other guiding-center following codes (ASCOT [10], OFMC [11]). The big difference between the SPIRAL and orbit code is that ORBIT uses the guiding-center approximation while the SPIRAL code follows the full gyro motion of the particles (at the expense of a significant increase of CPU time). After carefully examinations of the ORBIT and SPRIAL codes we conclude that the difference between the guiding-center and full orbit calculation is real and the finite gyro-radius is the cause of the increased losses [12].

Heat load estimates due to fusion-born alpha particles are important for a robust design of the ITER first wall and we have obtained those numbers from our simulations. In fact we have calculated the alpha particle heat load on the LCF instead of the wall which is 15 cm away in the vicinity of the plasma mid plane. Because the shape of the first wall is very similar to the LCF (except near the divertor region) we expect that the heat loads at the LCF are a good approximation for the wall heat loads. In figs. 5 and 6 are shown at the power losses at the LCF as function of toroidal and poloidal angle for scenario 2 and 4. Figs. 5a and 6a show the case without TBMs and in figs. 5b and 6b the TBMs are included. In the ripple only cases the head load is spread uniformly among 18 spots below the mid plane. with a maximum heat load of 20 kW/m^2 for scenario 2 and 100 kW/m^2 for scenario 4. Such heat loads are not threatening to the first wall.

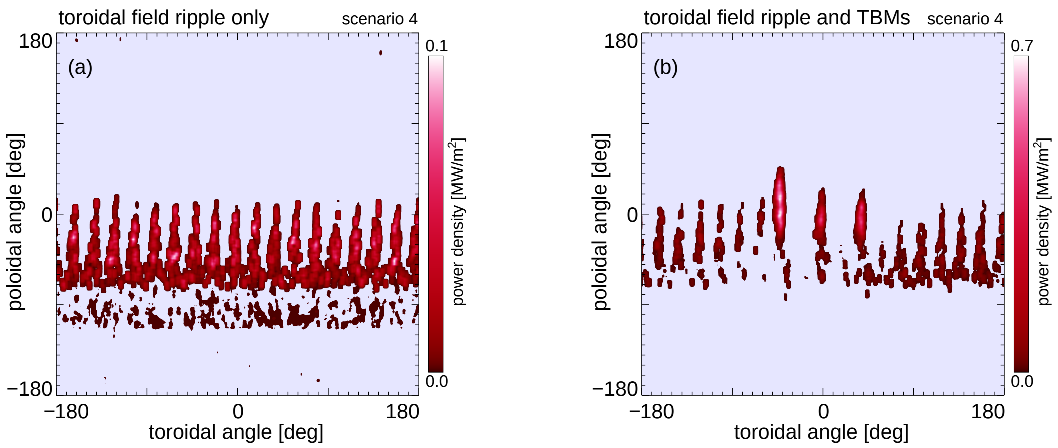

Figure 6: *calculated heat loads for scenario 4 at the LCF with field ripple only (a) and field ripple and TBMs (b). Note the seven fold increase in the power density scale for the TBM case.*

When the three TBMs are inserted three strongly localized hot spots appear in front of the TBMs whereby the first TBM at -40 deg. takes the majority of the power as can seen in figs. 5b and 6b. Maximum heat loads of 0.34 MW/m^2 were found for scenario 2 while in scenario 4 the maximum heat load reached 0.7 MW/m^2.

Comparing the heat loads of the alpha particles with the current design value for the first wall, 0.5 MW/m^2, reveals that the the heat loads for the toroidal field coil ripple only are well below the design value for both scenarios. In contrast, the localized losses due to the TBMs may pose a serious material risk to the first wall.

The alpha particle heat load is in addition to the heat loads from radiation and neutrons (up to about 0.2 MW/m^2). In our simulations we have only calculated alpha particle losses due to toroidal field ripple but additional alpha particle losses can be expected from MHD activity (such as Alfvén activity, fishbones, etc.) [13].

5 Conclusion and outlook

We have studied fusion born alpha particle losses that are caused by the (optimized) toroidal field ripple and by the extra field ripple due to three TBMs for two ITER scenarios. It was found that these losses and wall heat loads are within the limits for the first wall for the case without TBMs. The losses reported in this paper are higher than in comparable studies because we have used the full particle motion instead of the guiding center approximation. We have found that the finite Lamor radius of the alpha particles can cause a significant increase in the alpha particle losses. Details on this loss mechanism will be published soon [12].

When TBMs were introduced with their large ripple fields, the alpha particle losses increased significantly and very intense localized hot spots were found in front of the TBMs. The heat loads approached the ITER wall limit in the case of scenario 2 while in scenario 4 the loads are well above the design value of the first wall. The TBM ripple fields that were used in this study were not optimized to reduce the heat loads. Therefore, an engineering effort should be made to reduce the magnetic field ripple induced by the TBMs. Another option is to or add extra armor in front of the TBMs so that the first wall can withstand the increased heat loads.

In this study we have only investigated the ripple-induced fusion-born alpha particle losses. It is expected that plasma fluctuations such as MHD activity and turbulence will increase the losses [13]. Therefore, the alpha particle heat loads that we have found in this study are lower limits and the loads may increase when plasma fluctuation effects are taken into account.

Acknowledgments
This report was prepared as an account of work by or for the ITER Organization. The Members of the Organization are the People's Republic of China, the European Atomic Energy Community, the Republic of India, Japan, the Republic of Korea, the Russian Federation, and the United States of America. The views and opinions expressed herein do not necessarily reflect those of the Members or any agency thereof. Dissemination of the information in this paper is governed by the applicable terms of the ITER Joint Implementation Agreement. This work is supported by U.S. Department of Energy Contract No.DE-aC02-76-CHO3073.

References

[1] KONOVALOV, S.V., et al., Energetic Particle Ripple Loss in ITER, Proc. 28th EPS Conf. on Control. Fusion and Plasma Physics, (Funchal-Madeira, Portugal, 2001)

[2] TOBITA, K., et al., Plasma Phys. Control. Fusion **45** (2003) 133

[3] WHITE, R.B. and CHANCE, M.S., Phys. Fluids **27** (1984) 2455

[4] WHITE, R.B., The Theory of Toroidally Confined Plasmas, Imperial College Press, (2006)

[5] GRIBOV, Y., Plasma of ITER Scenario 2 (2006), and Plasma of ITER Scenario 4 (2006), ftp://pfctrl@ftp.jp.iter.org/array1/PF_control/EQDSK_files/Code PET/

[6] SABIENE, G., personal communication (2007) and CALCOLI, L.T., ROCHELLA, M., Ripple reduction using SS430 Fe inserts, Frascati, (2007)

[7] Arfken, G., Mathematical Methods for Physicists, Academic Press, (1970)

[8] HALL, G., and WATT, J.M. (Ed.), Modern Numerical Methods for Ordinary Differential Equations, Oxford University Press, (1976)

[9] FORD, B., and POOL, J.C.T., The evolving NAG Library Service. Sources and Development of Mathematical Software (Ed. Cowell, W.), Prentice-Hall, (1984) http://www.nag.com

[10] T. KURKI-SUONIO, et al., personal communication (2008)

[11] K. SHINOHARA, et al., personal communication (2008)

[12] G,J. KRAMER, G.J., WHITE, R.B., and NAZIKIAN, R., to be submitted (2008)

[13] FU, G.Y., and DAM J.W., Phys. Fluids **1** (1989) 1949